Mineralium Deposita (2024) 59:1737–1754
https://doi.org/10.1007/s00126-024-01291-2

ARTICLE

Petrogenesis of magmatic REE mineral occurrences near Jamestown, Colorado (U.S.A.)

Charles R. Stern[1] · Shea Burnham[1] · Andrew Kylander-Clark[2] · Julien Allaz[3] · Markus B. Raschke[4]

Received: 18 September 2023 / Accepted: 12 June 2024 / Published online: 12 July 2024

Abstract

Two magmatic REE-rich occurrences, located near Jamestown, Colorado, and hosted in the Precambrian Longs Peak granite batholith, exhibit unusual textures that suggest formation by fluoride-silicate melt immiscibility. Both contain small (<2 mm diameter) globular F-, P-, and REE-rich segregations of fluorite and monazite-(Ce). In addition, the northern of the two localities preserves evidence of a second melt immiscibility event in the form of larger (up to several cm diameter) aplite-hosted globular segregations of fluorite and the REE minerals allanite-(Ce), monazite-(Ce), fluorbritholite-(Ce), törnebohmite-(Ce), and cerite-(Ce). The southern of the two localities lacks these cm-scale globular textures, but instead contains much larger aggregates of these same REE minerals, with up to >57 wt. % ΣREE_2O_3, yet no fluorite, as well as large aggregates of allanite-(Ce) and quartz, and an amphibole-bearing REE-rich rock containing allanite-(Ce), other REE minerals, quartz and minor apatite. A new Nd-Sm laser ablation age of 1.422(24) Ga on monazite-(Ce) and allanite-(Ce) from the southern locality implies the same age of formation of 1.420(25) Ga as for the northern locality, with equally similar initial $\varepsilon_{Nd1.42Ga}$ values of these REE minerals. A newly discovered third locality, containing primarily allanite-(Ce), minor monazite-(Ce), and thorite, without fluorite, extends the number, spatial distribution and total volume of these mineralogically unusual magmatic REE occurrences. We suggest that the REE were concentrated in these three localities by multiple stages of fluoride-silicate melt immiscibility. For the southern locality, slower cooling of a possibly larger magma volume, or in a deeper environment, allowed greater aggregation of the immiscibly separated REE-rich phases, as well as loss of the volatile element F, resulting in a greater availability of Ca accommodated by the crystallization of amphibole and minor apatite.

Keywords Rare-earth-elements · Melt immiscibility · Fluorbritholite-(Ce) · Cerite-(Ce) · Törnebohmite-(Ce) · Allanite-(Ce) · Monazite-(Ce) · Rocky Mountains · Colorado

Introduction

The rare-earth-elements (REE) are critical metals, which, because of their unique magnetic, electronic, optical and quantum properties, are used in a variety of technological applications such as REE-magnets, lasers and lighting, and catalysts (Chakhmouradian and Wall 2012). The formation of REE deposits related to igneous rocks is a complex function of their igneous source, magmatic crystallization and fractionation processes, hydrothermal modification and supergene enrichment during weathering (Chakhmouradian and Zaitsev 2012; Smith et al. 2016: Vasyukova and Williams-Jones 2020). Understanding the sequence and relative role of these different magmatic processes is essential for understanding the formation of such deposits.

Here we discuss the multiple different magmatic process involved in the petrogenesis of two related concentrations

Editorial handling: C. N. Mercer

✉ Charles R. Stern
charles.stern@colorado.edu

✉ Markus B. Raschke
markus.raschke@colorado.edu

[1] Department of Geological Sciences, University of Colorado, Boulder, CO 80309, USA

[2] Department of Earth Science, University of California, Santa Barbara, CA 93106, USA

[3] Institute of Geochemistry and Petrology, ETH Zürich, 8092 Zürich, Switzerland

[4] Department of Physics, and JILA, University of Colorado, Boulder, CO 80309, USA

of REE minerals located approximately 1 km apart from each other in the pre-Cambrian rocks of the Rocky Mountain Front Range near Jamestown, Colorado (Fig. 1). Goddard and Glass (1940) originally suggested that cerite-(Ce) and allanite-(Ce) were the major REE minerals in these two localities. Allaz et al. (2015) described the northernmost locality in greater detail and determined that in fact fluorbritholite-(Ce) and allanite-(Ce) are the dominant REE minerals, with only a minor amount of cerite-(Ce) along with monazite-(Ce), bastnäsite-(Ce), and törnebohmite-(Ce). At this locality, these REE minerals occur in fluorite-rich globular segregations within white aplite dikes (Fig. 2a) that intrude along the contact between the Mesoproterozoic Longs Peak granite and bodies of Paleoproterozoic metasediments. Allaz et al. (2015) determined monazite-(Ce) and uraninite U-Th-Pb microprobe ages of 1.420(25) and 1.442(8) Ga, respectively, for the REE mineral segregations, suggestive of a co-genetic relationship with the host 1.420(30) Ga granite. However, Stern et al. (2018) subsequently showed that although the initial $\varepsilon_{Nd1.42Ga}$ values, ranging from -1.0 to -2.2 (average -1.6) for both the aplites and globular REE-rich segregations are similar to each other, they differ from the corresponding values for the granite and related granitic pegmatites, which range from -3.3 to

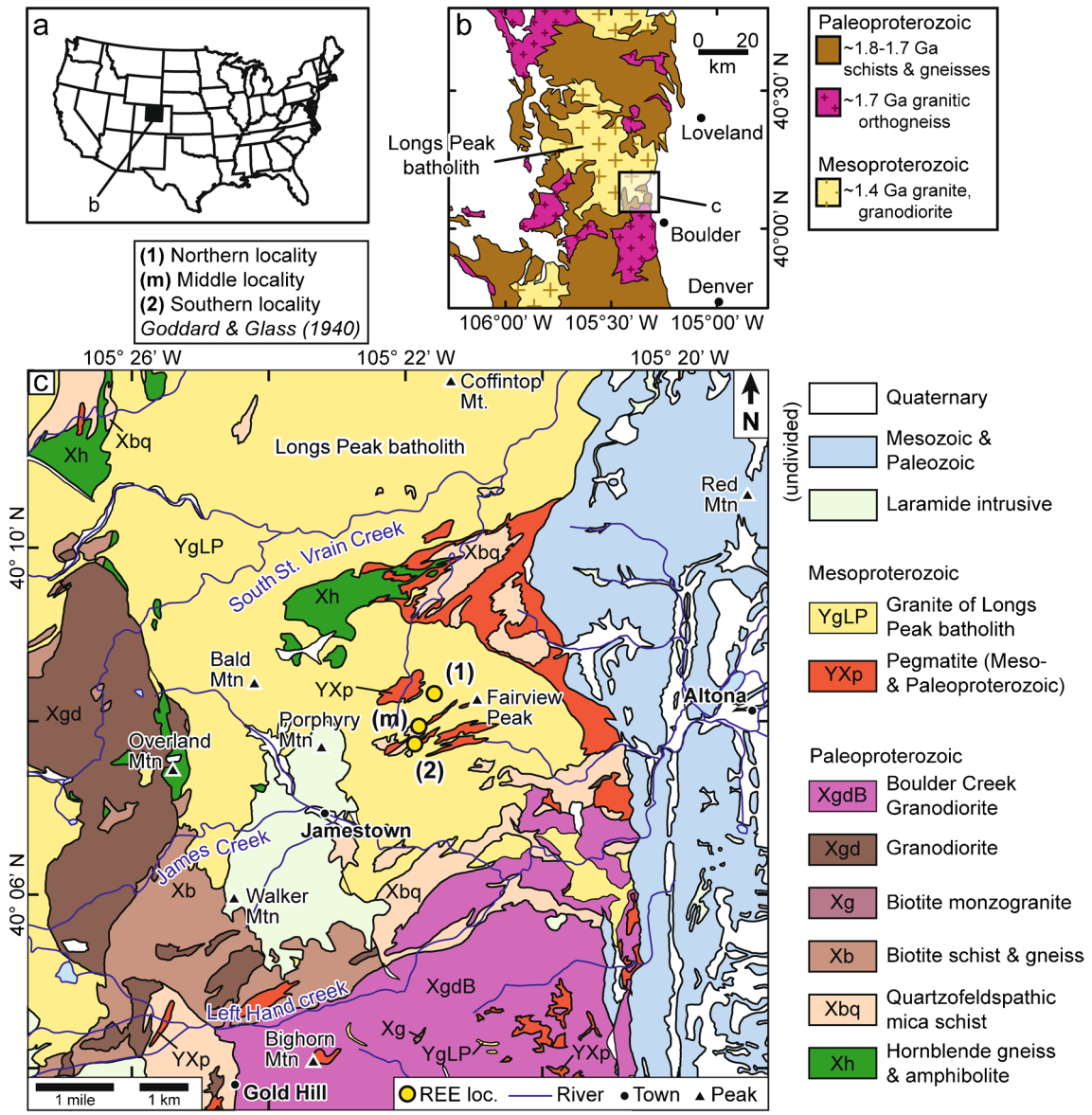

Fig. 1 Location maps modified from Allaz et al. (2015). **a** Map of the USA showing the location of map **b**. **b** General geological setting of the Mesoproterozoic intrusions within the Front Range of Colorado simplified after Tweto (1979). **c** Modified geological map from Cole and Braddock (2009), with locations of the northern (1) and southern (2) REE deposits originally described by Goddard and Glass (1940) and a new deposit (m) located between them

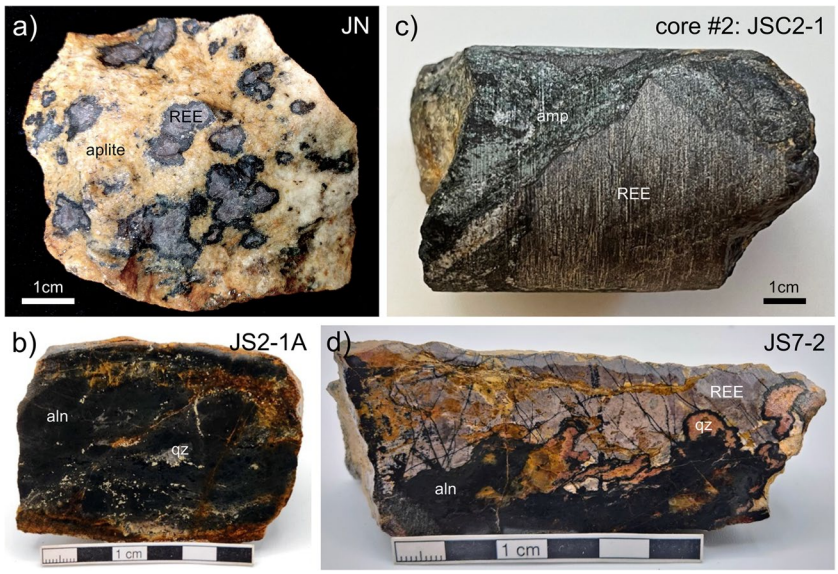

Fig. 2 Photographs of four texturally distinct REE-mineralized segregations, one (**a**) from the northern and three (**b, c** and **d**) from the southern of the two REE deposits described by Goddard and Glass (1940) near Jamestown, Colorado (Fig. 1). **a** Sample JN (Jamestown North), with dark REE-rich globular segregations within milky white aplite from the northern locality (#1 in Fig. 1). The segregations all consist of dark allanite-(Ce) rims surrounding somewhat lighter grey colored fluorbritholite-(Ce) + fluorite + monazite-(Ce) cores (Allaz et al. 2015). The aplite dominantly consists of plagioclase (Ab_{70-85}) along with lesser amounts of quartz, alkali feldspar and biotite (Stern et al. 2018). In this sample some of the small globular REE-rich segregations have agglomerated and coalesced into larger concentrations of REE-rich material. **b** Sample JS2-1A from the southern locality (#2 in Fig. 1) consisting of a dark black mass of allanite-(Ce) along with quartz and minor monazite-(Ce). **c** Sample JSC2-1 from core #2 (Fig. 3) in the southern locality. The sample contains both a greenish tinted rock consisting of amphibole, quartz and allanite-(Ce), and a lavender tinted aggregate of the REE minerals fluorbritholite-(Ce), monazite-(Ce), bastnäsite-(Ce), törnebohmite-(Ce), and cerite-(Ce). **d** Sample JS7-2 from the southern locality consisting of lavender tinted aggregate of the REE minerals fluorbritholite-(Ce), monazite-(Ce), bastnäsite-(Ce), törnebohmite-(Ce), and cerite-(Ce) cut by thin allanite-(Ce) veins above a mass of dark allanite-(Ce), and with small quartz-rich segregations surrounded by thin black allanite-(Ce) rims

-4.7 (average -3.9). The combination of these isotopic data, the globular textures of the REE-rich mineral segregations, and the relative distribution of the REE between these segregations and their host aplite, suggest that the REE-rich segregations formed by fluoride-silicate melt immiscibility following ascent, cooling, and decompression of what was initially a single homogeneous silicate magma. That magma, which intruded the granite, was derived from an isotopically distinct and possibly deeper more mafic source than that of the granite (Stern et al. 2018).

However, important differences are exhibited in the southern compared to the northern locality (Table 1), some of which were already noted by Goddard and Glass (1940). Most significantly, in the southern locality the aggregates of the same globally unique group of REE mineral are larger, up to several tens of centimeters in size, and they do not occur as globular segregations hosted in aplite (Figs. 2b, 2c and 2d), nor do they contain the large amount of fluorite characteristic of the northern locality. Therefore the role of fluoride-silicate melt immiscibility in the concentration of REE in this occurrence is uncertain.

Although the two occurrences described by Goddard and Glass (1940) are small in size and likely to be sub- or noneconomic, we present in this paper, as a contribution to the understanding of the complex sequence of magmatic processes involved in the concentration of REE, a detailed description of the southern locality in order to document the textural, mineralogical and chemical differences between the two localities (Table 1) and their implications for the different processes involved in the separation and concentration of the REE mineral segregations from their parental magmas. We also report on a newly discovered third locality (m in Fig. 1), situated between the two reported by Goddard and Glass (1940), which expands the spatial extent of these multiple, small, but mineralogically unusual magmatic REE-rich occurrences.

Geological setting

The two outcrops of REE minerals described by Goddard and Glass (1940) are spatially related to the Longs Peak granite batholith dated by Rb-Sr at 1.42(3) Ga (Peterman et al. 1968; Peterman and Hedge 1968; Anderson and Thomas 1985). The Longs Peak batholith was emplaced into the Paleoproterozoic metamorphic schists and gneisses (Xb,

Table 1 Summary of some of the similarities and differences between the northern and southern localities of REE mineralization near Jamestown

	Similarities:	Differences:	
		Northern locality	*Southern locality*
Age	1.421 (26) Ga		
Minerals	Allanite-(Ce), Monazite-(Ce)	Fluorite abundant	Fluorite scarce
	Fluorbritholite-(Ce)		Amphibole abundant
	Törnebohmite-(Ce)		
	Bastnäsite-(Ce)		
Lithologies	Small (<2 mm) globular F-, P-, and REE-rich segregations of fluorite and monazite-(Ce)	Globular REE-mineral segregations in fine-grained equigranular aplite	Separate units of massive REE-minerals and allanite-(Ce) segregations, an amphibole + REE minerals rock, and minor amounts of quartz-porphyritic felsic rock
Chemistry	REE-mineralization with >57 wt. % ΣREE_2O_3 and initial $\varepsilon_{Nd1.42Ga}$ =-1.6 (avg.)	Overall higher F and lower Fe content	Overall lower F and higher Fe contents
	Bulk mixtures of allanite-(Ce) and REE minerals with similar REE content and La/Yb ratios	Allanite-(Ce) with lower La/Yb ≃ 250, and REE mineral segregations with higher La/Yb ≃ 170	Allanite-(Ce) with higher La/Yb ≃ 1300 and REE mineral segregations with lower La/Yb ≃ 40
Genesis	Two stages of fluoride-silicate melt immiscibility concentrated REE	Rapid quenching preserved globular textures of immiscible F-, P- and REE-rich melts within aplite	Slow cooling allowed segregation of massive REE mineral and allanite-(Ce) aggregates, loss of F from the system and stabilization of amphibole
	Parental magmas derived from an isotopically similar source distinct from the source of the host Longs Peak granite		

Xbq, and Xh; Fig. 1) of the >1.7 Ga Idaho Springs Group at shallow depth (0.2–0.3 GPa; Anderson and Thomas 1985). The outcrops of REE minerals are located near the southeast edge of the Longs Peak batholith (Fig. 1), close to the margin of the intrusion (Goddard and Glass 1940), along the contacts between the granites of the batholith and bodies of metasedimentary biotite schists and gneisses (Xb and Xbq in Fig. 1) interpreted as roof pendants (DePaolo 1981; Selverstone et al. 2000). The Idaho Springs Group of metasedimentary rocks are reported to also include hornblende gneisses and amphibolite-bearing schists (Xh in Fig. 1) as well as biotite schists, but these have not been observed in the immediate vicinity of the deposits of REE minerals. Neither do any carbonate rocks occur in this area.

The Longs Peak granite batholith and other so-called Silver Plume-type Mesoproterozoic intrusions in Colorado are a series of anorogenic (A-type) two-mica monzogranites to syenogranites exhibiting enrichment in K and other incompatible elements (Rb, Sr, REE), and depletion in Ca and Mg compared to orogenic granites (Boos and Boos 1934; Wells 1967; Flanagan 1973; Baker et al. 1976). Al_2O_3/($CaO+Na_2O+K_2O$) molecular ratios are 1.0 to 1.3, hence their classification as peraluminous granites (Anderson and Thomas 1985). Their overall geochemistry suggests that the source of these intrusions was the melting of garnet-rich high-grade quartzo-feldspathic continental crust (DePaolo 1981; Anderson and Thomas 1985). In terms of REE content, limited data suggest a strong enrichment in light REE (50–500 times primitive mantle values) and a strong fractionation of light relative to heavy REE, with La/Yb >25, consistent with a garnet-bearing source (Flanagan 1973; Baker et al. 1976). Nd-isotopic data for the REE mineralized rocks from the northern locality (initial $\varepsilon_{Nd1.42Ga}$ values ranging from -1.0 to -2.2 with an average of -1.6) suggest that these crystallized from a magma derived from a more mafic and isotopically distinct source than that of the Longs Peak granite (initial $\varepsilon_{Nd1.42Ga}$ values ranging from -3.3 to -4.7 with an average of -3.9), located perhaps deeper in the lower crust or upper mantle (Stern et al. 2018).

Sample sites

The geology and petrochemistry of samples from the northern locality have been described in detail by Allaz et al. (2015) and Stern et al. (2018). The southern locality, originally described as an outcrop by Goddard and Glass (1940), was turned into a 5 m wide and 3 m deep pit as part of uranium exploration efforts in the 1950's, and deepened to ca. 5 m to follow and further expose the REE minerals as part of this project (Fig. 3). The 26 rocks analyzed for chemical composition (ESM1) were selected after examination of thin sections cut from a much greater number of samples. These include samples of dump material (11) from the original excavation, outcrop samples (12) collected from the walls and floor of the pit, and samples (3) from three ~1 m long cores drilled into the floor of the pit.

Samples analyzed from the eastern wall of the pit include four Idaho Springs Group metasedimentary biotite schists with varying amounts of micaceous and quartzo-feldspathic components (Fig. 3; ESM1). They also include two (JS4-6 and JS4-8; ESM1) REE-rich amphibole-bearing rocks which appear to have intruded roughly along the foliation of the schists. No REE-poor hornblende gneisses, which do occur elsewhere within the Idaho Springs Group metamorphic rocks (Xh in Fig. 1), were found within either wall of the pit. All the amphibole-bearing samples studied, which were also collected from the dump material (JS2-1; ESM1) and two of the three cores (JSC2-1, JSC2-5B, and JSC3-2; ESM1) at the site, contain allanite-(Ce) and quartz, as well as in some cases segregations of other REE minerals and minor fluorite, but no feldspars, and are considered to be a significant component of the REE mineral occurrence.

The eastern wall of the pit also contains rocks with large quartz porphyroblasts, or possibly phenocrysts, in a fine-grained granular matrix of quartz and feldspar. As discussed in more detail below, these rocks, three of which were analyzed (JS3-2a, JS3-4b and JS4-1; ESM1), may belong to the Idaho Springs Group metasediments, but alternatively, may be genetically related to the REE-rich rocks, although they do not host the REE mineralized rocks themselves and differ petrochemically from the aplites found in the northern locality.

The western wall of the pit is composed of both metasedimentary schists and what Goddard and Glass 1940; Fig. 3a) mapped as "pegmatite and aplite." However, this "aplite" is actually a relatively fine-grained phase of the Longs Peak two-mica granite, and is petrochemically distinct from the white aplite that hosts the REE mineral segregations in the northern locality (Fig. 2a). The "pegmatite" is a somewhat coarser grained two-mica Longs Peak granite, but not as coarse grained or quartz-rich as many pegmatite bodies in the area. We consider the "pegmatite and aplite" mapped by Goddard and Glass (1940) to simply be finer and coarser grained varieties of the Longs Peak granite (Fig. 3b). Three samples of these granites (ESM1) collected from the western wall of the pit were analyzed. Some REE-rich rocks also occur along the western wall of the pit intermixed with felsic rocks that may belong to the Idaho Springs Group or, alternatively, be associated with the REE mineralization.

Three short drill cores at the base of the pit contain REE minerals both with and without amphibole (Fig. 3c), as well as unequivocal Idaho Springs Group metamorphic rocks, granite, and felsic rocks that may be either metamorphic or genetically related to the REE minerals. Three samples (JSC2-1, JSC2-5B, and JSC3-2; ESM1) were analyzed of

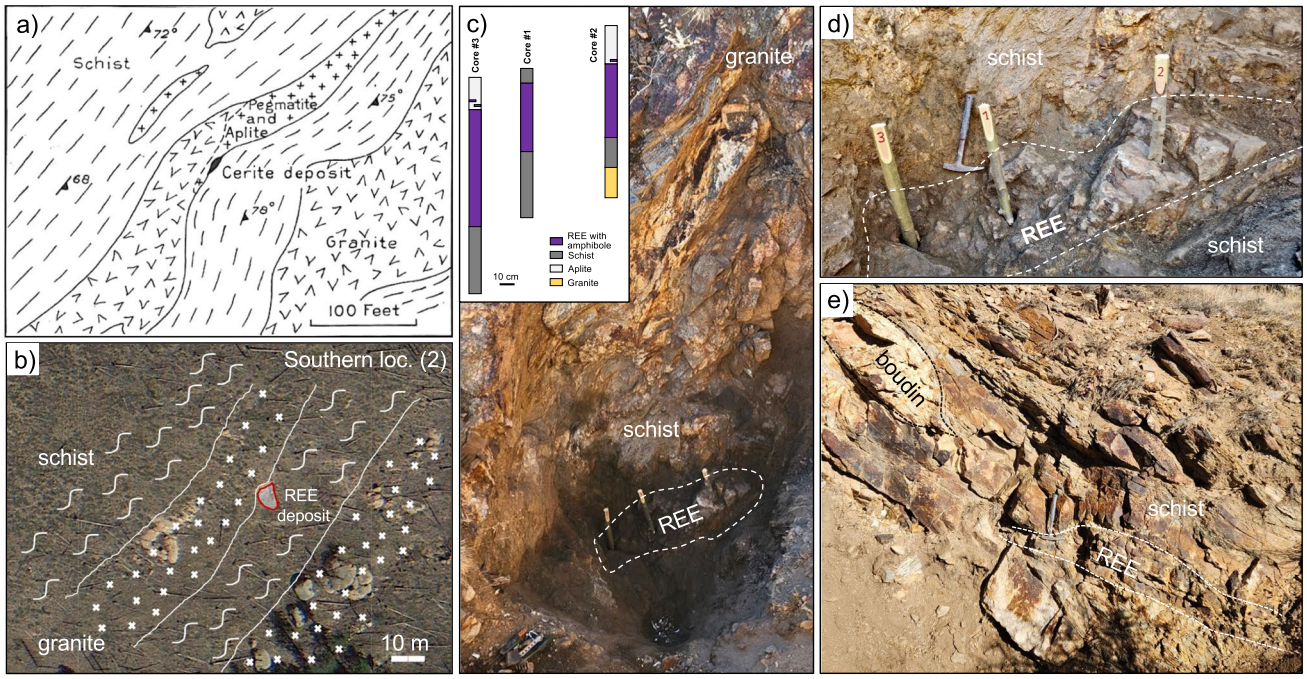

Fig. 3 **a** Geologic map from Goddard and Glass (1940) of the southern (#2 in Fig. 1) of what they considered to be two cerite deposits, both located along the contact between granite and schist. **b** An updated map showing the details of the geology superimposed on a google satellite image around this same locality located at North 40.12910, West -105.36441. **c** Photograph of the western wall of the pit dug at the southern REE mineralization locality (#2 in Fig. 1), consisting dominantly of metasedimentary mica schists and quartzo-feldspathic rocks, and the location of three short drill cores taken from the REE-rich pod at the base of the pit. Inset illustrates the lithologies encountered in these three drill cores. **d** Photograph of the three drill holes at the base of the pit, each hole approximately 1 meter deep, from which REE mineralized samples were collected. **e** Photograph of the eastern wall of the pit, consisting dominantly of metasedimentary mica schists and both thin layers and a large boudin of quartzo-feldspathic rocks intruded roughly along the foliation of the schists by an REE-rich pod. REE mineralized samples from this side of the pit were collected from between the red lines

amphibole-bearing rocks from the cores. Also analyzed by EMP for mineral chemistry (ESM2) were two surface samples of allanite-(Ce) along with minor monazite-(Ce) and thorite from a previously unreported 2 m by 2 m outcrop located ~150 m north of the southern locality (location m in Fig. 1).

Analytical methods

Bulk-rock major and trace-element compositional analyses (Table 2; ESM1) were obtained from Activation Labs Inc. (Ontario, Canada). The analysis of major elements was conducted by fusion ICP, and trace elements by ICP (Ba, Be, Sc, Sr, V, Y, Zr) or ICP-MS (REE and other trace elements). Fluorine was measured by the ion-selective electrodes method. For the graphical comparison of the REE contents of the different rock types (Figs. 5 and 8), the REE values were normalized to those of primitive mantle pyrolite (La=0.648, Ce=1.675, Pr=0.254, Nd=1.250, Sm=0.406, Eu=0.154, Gd=0.544, Tb=0.099, Dy=0.674, Ho=0.149, Er=0.438, Tm=0.068, Yb=0.441, Lu=0.068).

Mineral analyses (ESM2 Tables 1-4) were performed on multiple samples, multiple grains in each sample and multiple points within each grain using a JEOL JXA-8230 electron microprobe at the University of Colorado-Boulder. Operating conditions using a W-cathode were 15 keV, and either 20 nA beam current and a 5 µm defocused beam for amphibole and biotite, or 30 nA and a focused beam for allanite-(Ce) and monazite-(Ce). The complete analytical setups for amphibole, allanite-(Ce) and monazite-(Ce) are summarized in ESM3 Tables 1 and 2, including the list of peak interference corrections for these REE-minerals. Olivine, labradorite and amphibole were used as secondary samples to constrain the accuracy of the major element oxides, and allanite-(Ce) samples SL1-1, SL1-7 and REE9, bulk samples of which had been analyzed by Activation Labs (ESM1), were used as secondary standards to evaluate the accuracy of the EMP analysis of the trace-element in samples of allanite-(Ce) from these sample rocks.

Isotopic analyses ($^{143}Nd/^{144}Nd$ and $^{147}Sm/^{144}Nd$ ratios; ESM4) were conducted by LA-ICP-MS at the University of California Santa Barbara, using a Nu Plasma 3D multi-collector ICP-MS coupled to a Photon Machines Excite 193 nm laser ablation system. Three samples (JS4-8, JS1-2, and

Table 2 Average compositions of the various lithologies in the REE-rich magmatic deposits near Jamestown, Colorado

Rock type	Granite	REE-rich aggregates		Allanite rims and rocks		REE-rich aggs + allanite rims		Amph rocks	Aplites		Bulk rock**
Location*	N & S	south	north	south	north	south	north	south	south	north	north
# of samples	9	4	3	3	4	2	core 55% rims 45%	7	3	5	5
SiO_2	72.90	20.80	18.60	32.70	34.30	27.60	25.60	54.10	74.70	68.20	63.30
TiO_2	0.26	0.01	0.00	0.61	0.13	0.03	0.09	0.02	0.01	0.03	0.07
Al_2O_3	14.30	0.92	0.32	11.10	14.10	4.82	5.98	4.49	12.00	18.30	16.30
Fe_2O_3(T)	1.87	2.08	0.32	19.00	11.80	7.40	6.21	13.90	1.19	3.78	2.67
MnO	0.03	0.32	0.30	0.65	0.89	0.35	0.53	0.75	0.08	0.02	0.16
MgO	0.35	0.16	0.02	0.67	0.65	0.69	0.31	6.64	0.68	0.13	0.53
CaO	0.44	7.76	14.30	6.92	9.10	3.27	11.70	9.06	3.28	2.86	4.42
Na_2O	1.75	0.03	0.02	0.10	0.22	0.06	0.09	0.28	3.04	5.56	3.75
K_2O	5.47	0.05	0.03	0.12	0.09	0.08	0.06	0.18	0.42	1.51	0.68
P_2O_5	0.24	4.26	4.66	1.06	1.72	4.19	3.31	0.68	0.03	0.15	0.46
F	0.16	1.70	6.85	0.16	0.34	0.83	3.91	1.43	0.22	0.16	0.47
S	0.01	-	-	-	-	-	-	1.25	1.87	-	-
ΣREE_2O_3	0.03	57.14	51.39	25.05	24.65	47.01	39.35	6.25	0.11	0.20	5.29
LOI	1.72	3.92	3.91	1.56	1.56	3.22	2.71	2.12	1.31	1.03	1.91
Total	99.53	99.25	99.72	99.49	99.55	99.44	99.85	101.45	98.42	101.93	100.01
PPM data											
Cs	6	0.7	0.5	0.9	0.5	1.0	0.7	1.0	1.0	1.8	1.3
Rb	364	3.3	2.0	11	8	9	5	10	43	44	86
Ba	347	39	90	21	221	160	127	131	675	870	1185
Sr	82	405	2133	290	731	264	1440	246	564	1900	1866
Nb	41	1	1	10	8	4	4	2.7	0.9	3.4	8.9
Zr	165	14	31	55	11	59	25	36	105	35	40
Y	24	23770	9472	795	3630	10097	6573	3263	21	41	802
Hf	4	30	10	2.0	4.4	13	7	9.2	5.2	1.0	1.5
Th	30	4235	3230	1384	1223	3210	1456	612	3.2	13	359
Pb	36	3745	1960	446	777	2615	1453	774	29	93	-
U	5	4238	4113	282	923	3555	2300	954	7.2	33	238
La	51.8	44225	77033	47500	40060	59700	60973	6183	74.6	434	8165
Ce	120.7	183750	221333	109633	102173	177500	168929	23257	142	799	20694
Pr	15.1	31975	26100	11203	12507	24750	19915	4144	23.5	126	2665
Nd	57.2	144000	97300	32400	42380	95300	72206	20556	80.8	445	9112
Sm	10.1	26050	12200	2533	5133	14300	8857	3911	9.46	54.4	1068
Eu	0.81	5755	2460	346	1004	2180	1743	829	2.34	14.4	224
Gd	5.37	12275	5313	594	2098	6175	3726	2026	4.49	27.6	563
Tb	0.74	1248	537	53	218	574	378	205	0.59	2.85	52.3
Dy	4.05	5408	2257	196	876	2420	1572	857	3.61	12.0	200
Ho	0.77	814	333	25.6	119	330	226	109	0.70	1.65	22.9
Er	2.20	1670	751	58.6	257	712	485	253	2.15	3.85	48.4
Tm	0.35	201	86.0	7.23	29.7	80.5	58.6	26.7	0.31	0.44	6.11
Yb	2.22	1100	463	40.7	160	445	316	149	2.09	2.33	34.3
Lu	0.31	148	57.8	5.78	21.3	56.1	39.9	19.1	0.33	0.29	3.81
La/Yb	23	42	166	1297	250	137	193	41	33	186	162

*Data for the northern locality from Stern et al. (2018).

**Bulk-rock sample of aplite and globular REE-rich segregations which together represent the hypersolvus parental magma prior to their separation by fluoride-silicate melt immiscibility (Stern et al. 2018).

JS1-9) were chosen for analysis of selected monazite-(Ce) and allanite-(Ce) grains. The number of spots analyzed per grain ranged from 6-30, depending on the size of the grain. Amphibole grains were also analyzed in rock sample JS4-8, but the amphibole grains did not yield high enough Nd-Sm concentrations to obtain useful results. Sample JS1-2 has a high concentration of REE minerals, including both monazite-(Ce) and allanite-(Ce) and four allanite-(Ce) and three monazite-(Ce) grains were analyzed. Sample JS1-9 contains primarily allanite-(Ce) with some quartz and monazite-(Ce) and three allanite-(Ce) and one monazite-(Ce) grains were analyzed.

Instrument conditions are outlined in Kylander-Clark (2010). Both allanite (35 µm) and monazite (20 µm) were run at 10 Hz for 15 s, following a 50 s baseline. Neodymium isotope data were normalized using an exponential mass bias correction and a natural $^{146}Nd/^{144}Nd$ ratio of 0.7219. The isobaric interference of ^{144}Sm on ^{144}Nd was corrected by measuring the $^{147}Sm/^{149}Sm$ ratio, calculating a mass-bias correction (assuming a natural ratio of 147/149 = 1.0868), and calculating the signal of ^{144}Sm, using a ratio of 144/149 = 0.22332. These corrections were performed using a data reduction scheme created in Iolite v2.5 (Paton et al. 2010). Secondary reference materials (RMs) were analyzed as control samples: Trebilcock (accepted value: 0.512616) and Mae Klang (0.512646) monazites, JNdi+REE glass (0.512098), Durango (0.512489) and Aber (0.511188) apatites and Daibosatsu allanite (0.512599) (Foster and Vance 2006; Fisher et al. 2011). All RMs yielded values within the uncertainties of their accepted values: Trebilcock: 0.512625 ± 0.000026 (n = 10, MSWD = 3.5); MaeKlang: 0.512622 ± 0.000036 (n = 9, MSWD = 4.6); JNdi+REE glass: 0.512093 ± 0.000045 (n = 10; MSWD = 0.29); Durango: 0.51252 ± 0.00012 (n = 9, MSWD = 0.35); Aber: 0.511219 ± 0.000088 (n = 9; MSWD = 0.88); Daibosastu: 0.512570 ± 0.000053 (n = 9; MSWD = 3.5).

Sample Petrochemistry

Metamorphic rocks

Idaho Springs Group metasedimentary rocks collected from the eastern wall of the pit include dark colored biotite schists with quartz, plagioclase and K-feldspar (JS4-10; Figs. 4a and 4c) and quartzo-feldspathic rocks with minor amounts of both biotite and muscovite (JS3-8; Figs. 4b and 4d). The east wall of the pit also contains a prominent large boudin of feldspar-rich Idaho Springs Group metamorphic rock (JS6-2; Fig. 3e). Similar metasedimentary rocks occur in the vicinity of the northern REE mineralization locality (Goddard and Glass 1940; Allaz et al. 2015; Stern et al. 2018). Biotites in all these samples are dark brown, have FeO >20 wt %, TiO_2 >2 wt. % and MgO <9 wt. % (ESM2 Table 1), and in places contain zircons with radiation damage halos. Bulk whole-rocks chemistry of four samples (EMS1) are highly variable, consistent with the significant differences in their modal mineral abundances. These rocks have moderate K_2O >2 wt. % and Rb >150 ppm contents reflecting small amounts of modal K-feldspar and muscovite among their constituent minerals. Two of the schist samples have negative Ce anomalies as does one from the northern locality (Fig. 5a).

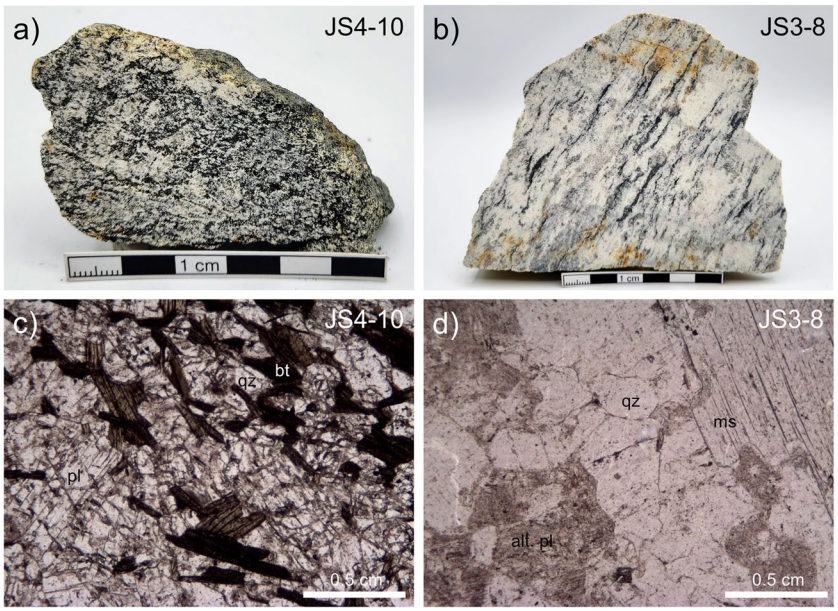

Fig. 4 **a** Biotite schist sample JS4-10 from the west wall of the pit. **b** Quartz-rich schist samples JS3-8 from the east wall of the pit. **c** and **d** Photomicrographs of these same two metasedimentary rocks. (bt = biotite; qz = quartz; ms = muscovite; pl = plagioclase; alt. pl = altered plagioclase)

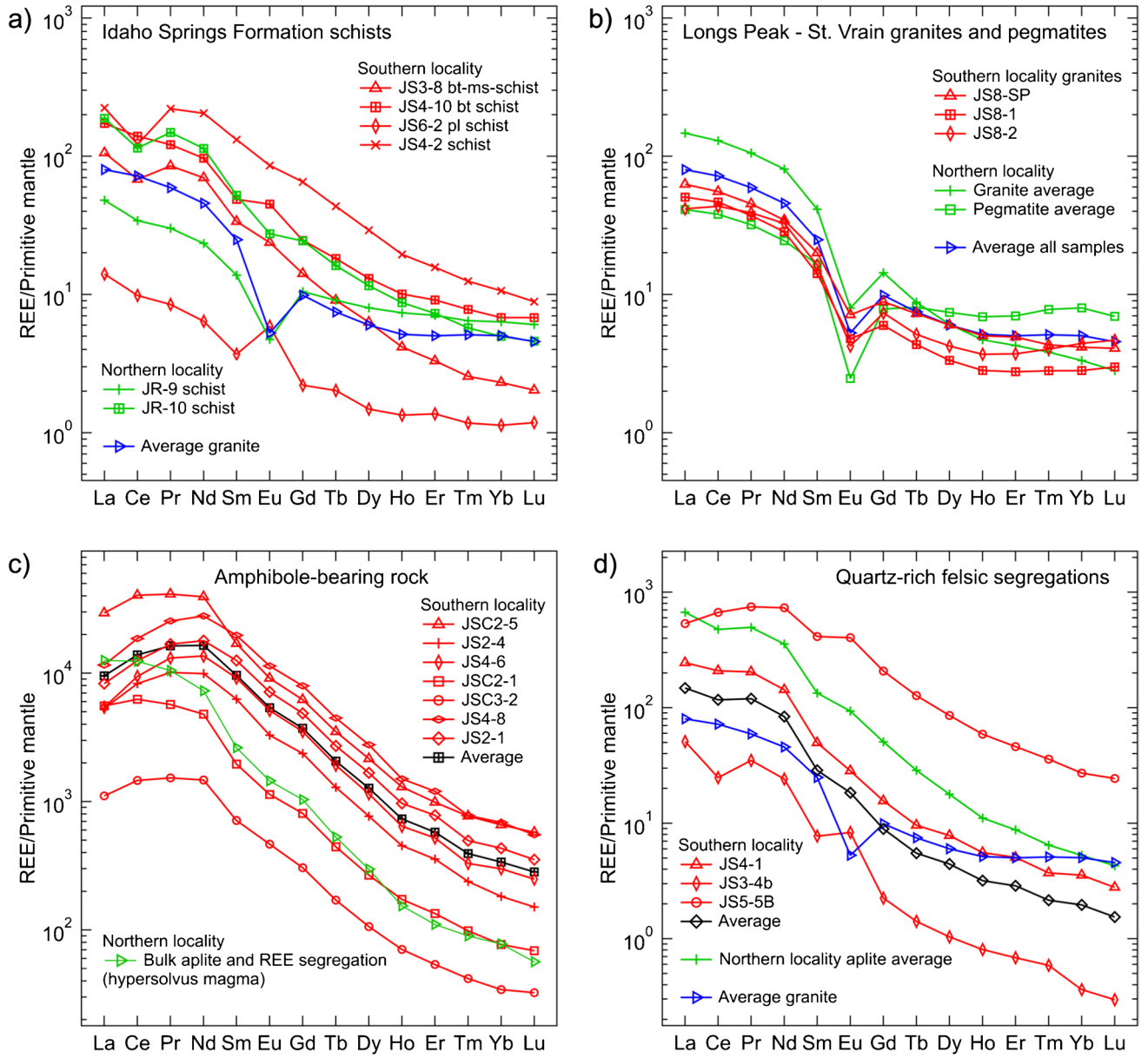

Fig. 5 REE contents, normalized to primitive mantle. **a** Four bulk whole-rock samples of Idaho Springs Group Proterozoic schists from the southern locality (red; ESM1) and two from the northern locality of REE minerals, compared to the average of nine samples of Longs Peak granite (blue; Table 2). **b** Three bulk whole-rock samples of Longs Peak granites and pegmatites (red; ESM1) from the southern locality compared to the average of samples of granite and pegmatite from the northern locality (green; ESM1), and the average of all nine samples from both localities (blue; Table 2). **c** Six bulk whole-rock samples of amphibole-bearing rocks (red; ESM1), and their average composition (black; Table 2) compared to the parental magma for the REE mineralized rocks in the northern locality (green; Table 2). **d** Three felsic rocks from the southern locality (ESM1), and their average (black; Table 2) composition compared to that of the aplites from the northern locality (green; Table 2)

Granites

Longs Peak granites from the vicinity of the southern locality include, to the southeast, a porphyritic variety with K-feldspar (orthoclase partially converted to microcline) phenocrysts in a fine-grained groundmass of quartz, plagioclase, brown biotite and muscovite mica, and accessory apatite, zircon and opaque minerals. This is the most common and distinctive textural type of granite within the Longs Peak granite batholith. Along the western margin of the REE occurrence a texturally more variable granite, mapped as "aplite and pegmatite" by Goddard and Glass 1940; Fig. 3a), consists of a mixture of fine and coarse grained two-mica equigranular granites (Fig. 3b). Bulk whole-rock chemistry

of one sample of K-feldspar porphyritic granite (JS8-SP) and two coarse grained granite samples (JS8-1 and JS8-2; ESM1; Fig. 5b) are similar to each other and to samples of Longs Peak granites and pegmatites from the vicinity of the northern locality. Brown biotites in all these granitic samples have FeO >20 wt. %, TiO_2 >2 wt. % and MgO <7 wt. % (EMS2 Table 1). The granites have, on average (Table 2; ESM1), higher K_2O and Rb than the metamorphic rocks they intrude reflecting their greater proportion of modal K-feldspar and muscovite. They also have on the average light REE enrichment of ~100 times primitive mantle (Fig. 5b) and La/Yb ~25. These values are similar to other Silver Plume-type anorogenic (A-type) two-mica granites in Colorado (Flanagan 1973; Baker et al. 1976; Anderson and Thomas 1985).

REE mineralized samples

The REE mineralized samples we studied include three visually and mineralogically different lithologies (Fig. 2); 1) a massive lavender colored fine-grained aggregate of REE minerals (Fig. 2d); 2) dark black masses of allanite-(Ce) along with quartz and minor monazite-(Ce) (Fig. 2b); and 3) greenish tinted rocks consisting of amphibole, quartz, allanite-(Ce), apatite, and variable amounts of other REE minerals (Fig. 2c).

Lavender REE mineral aggregates

These aggregates (Fig. 2d) consist of fine-grained REE minerals identified as fluorbritholite-(Ce), along with monazite-(Ce), bastnäsite-(Ce), törnebohmite-(Ce), cerite-(Ce) and uraninite based on qualitative electron microprobe energy dispersive element scans (Fig. 6) as well as quantitative wave dispersive analysis. This REE mineral assemblage is similar to the central part of the globular segregation of REE minerals in the northern locality (Fig. 2a; Allaz et al. 2015). However, in contrast to the northern locality, fluorite is scarce or absent in the southern locality (Table 1). Also, at least one Y-rich REE silicate mineral that does not occur in the northern locality occurs in the southern locality. The aggregates are commonly rimmed by allanite-(Ce), monazite-(Ce) and granular quartz margins (Figs. 2d and 6) and cut by quartz and/or allanite-(Ce) veins and/or fine-grained aplite dikelets consisting of quartz, plagioclase, and monazite-(Ce). However, they are not hosted in aplite as are the globular segregations in the northern locality (Fig. 2a). Also, the REE mineral zonation in the southern locality is more irregular compared to that from the north (Fig. 6; Allaz et al. 2015). Significantly, these REE mineral-bearing aggregates from the southern locality contain sporadically distributed small (<2 mm in diameter) rounded globular aggregates of fluorite and monazite-(Ce) (Fig. 7), similar to those described from the northern locality (Table 1; Allaz et al. 2015; Stern et al. 2018), suggesting the occurrence of an immiscible separation of an F-, P-, and REE-rich liquid prior to the crystallization of the fine-grained REE minerals in the larger lavender aggregates.

The lavender aggregates of REE minerals in the southern locality have an average of 2.1 wt. % Fe_2O_3, fluoride contents of 1.7 wt. %, and CaO of 7.9 wt. % (Table 2; ESM1). These are all notably different from the northern locality samples (Table 1), which have lower average Fe_2O_3 of only 0.5 wt. %, but much higher fluoride content of 9.3 wt. % and CaO content of 17.5 wt. %

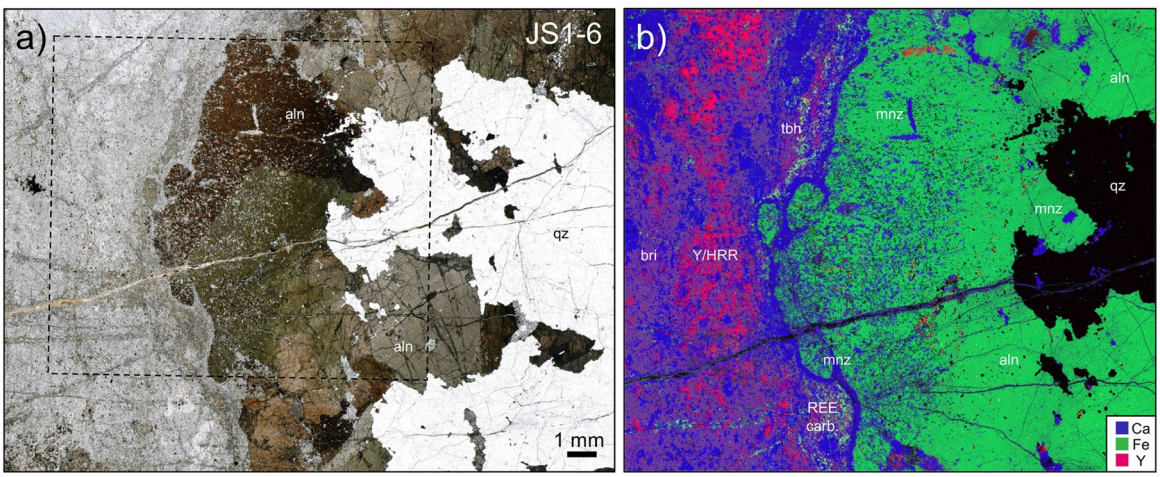

Fig. 6 **a** A photomicrograph, and **b** an energy-dispersive element scan (green = Ca; blue = Ce; red = Y) of a section of sample JS1-6 containing quartz, allanite-(Ce), monazite-(Ce) and an aggregate of other REE minerals including fluorbritholite-(Ce), bastnäsite-(Ce), törnebohmite-(Ce), and an as yet unidentified Y- and HREE-rich silicate. Mineral identifications were made by quantitative wave-dispersive analysis. (mnz = monazite-(Ce); aln = allanite-(Ce); bri = fluorbritholite-(Ce); tbh = törnebohmite-(Ce); REE-carb = bastnäsite; Y/HREE = unidentified Y- and HREE-rich silicate phase)

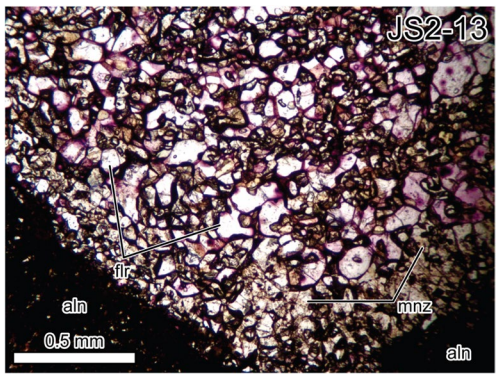

Fig. 7 Photomicrograph of an example of the small (<2 mm in diameter) fluorite and monazite globular clusters observed in both the southern (sample JS2-13) and northern localities. (flr = fluorite)

(Table 2; Stern et al. 2018), consistent with the different modal abundance of fluorite between the two localities (Table 1). This marks an important difference between the two localities, as Stern et al. (2018) suggested that fluorine, along with phosphate, played a key role in separating, by liquid immiscibility, the REE-rich globular segregations from the aplite in the initially homogeneous magma at the northern locality. The REE contents of the REE mineral aggregates in the southern locality (Fig. 8a; ESM1) also have more curved normalized REE patterns, with lower La, but higher middle and heavy REE, and much lower La/Yb ratios than the REE-rich globular segregations in the northern locality.

Dark allanite-(Ce) rich rocks

Allanite-(Ce) occurs both as thin veins within and thin rims on the margins of the massive lavender aggregates of REE-minerals described above (Fig. 2d), but also as large black nodules of allanite-(Ce) and quartz (Fig. 2b) with minor monazite-(Ce). In contrast, such large aggregates of allanite-(Ce) have not been observed in the northern locality. Quartz in the nodules occurs as large >3 cm crystals and also as concentrations of much smaller granular grains along with sulfides.

Bulk whole-rock analyses of the allanite-(Ce) in the massive nodules have an average of 19.0 wt. % Fe_2O_3, 11.1 wt. % Al_2O_3 and 6.9 wt. % of CaO, compared to 13.3 wt. % Fe_2O_3, 17.5 wt. % Al_2O_3 and 9.7 wt. % CaO in the allanite-(Ce) rims of the globular REE-rich segregations in the northern locality (Table 2; ESM1). The average composition of allanite-(Ce) determined in nine samples by electron microprobe is similar to the bulk whole-rock analyses (ESM2 Table 2), but with somewhat lower SiO_2 and P_2O_5 because the bulk whole-rock samples also contain some quartz and monazite-(Ce). Although not spatially consistent, the microprobe analyses show some range of variation both between samples and within individual grains. In contrast, allanite-(Ce) in the rims of the REE-rich globular segregations in the northern locality are spatially zoned (Allaz et al. 2015), with an outer Zone #1 consisting of green allanite-(Ce), with relatively low total Fe_2O_3 <12 wt. % and high Al_2O_3 >17 wt. % contents, and a thinner inner Zone #2 consisting of brown allanite-(Ce), with higher total Fe_2O_3 >14 wt. % and lower Al_2O_3 < 15 wt % content, and monazite-(Ce). The bulk whole-rock

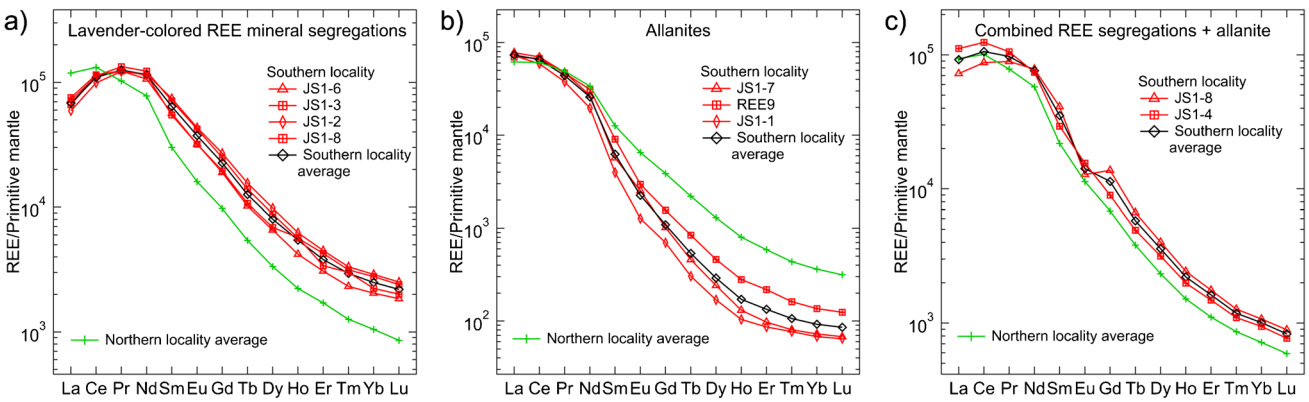

Fig. 8 REE content, normalized to primitive mantle. **a** Four bulk whole-rock samples of massive lavender colored REE mineral aggregates (red; ESM1) and their average (black; Table 2) compared to the average of the cores of bulk whole-rock globular clusters of REE minerals (Fig. 2a) from the northern locality (green; Table 2). **b** Three bulk whole-rock samples of dark black allanite-(Ce) rich aggregates (red; ESM1), and their average (black; Table 2) compared to the average of allanite-(Ce) samples from the rims of the REE-rich globular segregations in the northern locality (green; Table 2). **c** Two samples of bulk whole-rock mixtures of lavender colored REE mineral segregations and allanite-(Ce) from the southern locality (red; ESM1), and their average (black; Table 2) compared to calculated values for similar bulk mixtures of the rim and core of REE-rich globular segregations from the northern locality (green; Table 2)

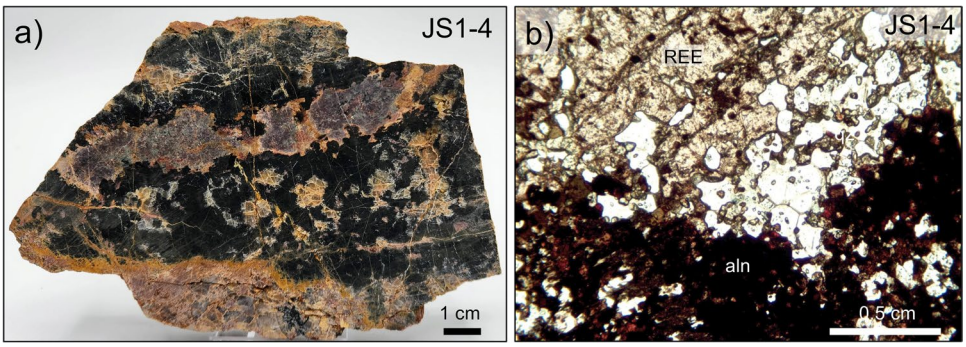

Fig. 9 **a** Photo and **b** photomicrograph of lavender colored REE mineral segregations and allanite-(Ce) mixtures in sample JS1-4

composition of the dark brown allanite-(Ce) aggregates in the southern locality are more similar to the composition of the brown allanite-(Ce) in Zone #2 forming the inner rims of the REE-rich globules in the northern locality.

The allanite-(Ce) in the dark nodules of the southern locality have similar light REE contents but much lower heavy REE contents that the allanite-(Ce) rims around the globular REE segregations from the northern locality (Fig. 8b; Table 1), and therefore much higher La/Yb ratios than allanite-(Ce) in the northern locality (Table 2). Analysis of bulk mixtures of the lavender REE mineral aggregates and allanite-(Ce), including one sample (JS1-4) in which they are crystallized together (Fig. 9) and one sample of lavender REE mineral aggregate and its allanite-(Ce) rim (JS1-8), have average REE contents and La/Yb ratios similar to bulk mixtures of globular REE-rich segregations and allanite-(Ce) rims from the northern locality (Fig. 8c; Tables 1 and 2; EMS1). This reflects the combination of the relatively high Yb content and low La/Yb ratios of the lavender REE mineral aggregates in the southern locality being balanced by the much lower Yb content and higher La/Yb of the allanite-(Ce) in this locality. The average total Fe_2O_3 of these bulk mixtures are higher in the southern locality, but their CaO and F contents are much lower compared to the northern locality reflecting the scarcity of fluorite in the southern locality.

Green-tinted amphibole-bearing rocks

Green-tinted REE-rich amphibole-bearing rocks, which are not found in the northern locality, consist of equigranular amphibole, allanite-(Ce), and quartz, along with minor apatite and fluorite, and variable amounts of lavender REE mineral segregations containing fluorbritholite-(Ce), monazite-(Ce), bastnäsite-(Ce), törnebohmite-(Ce), cerite-(Ce) and uraninite (Fig. 10). These REE mineral segregations are commonly surrounded by allanite-(Ce) rims, but are not globular in shape. In some samples the amount of lavender

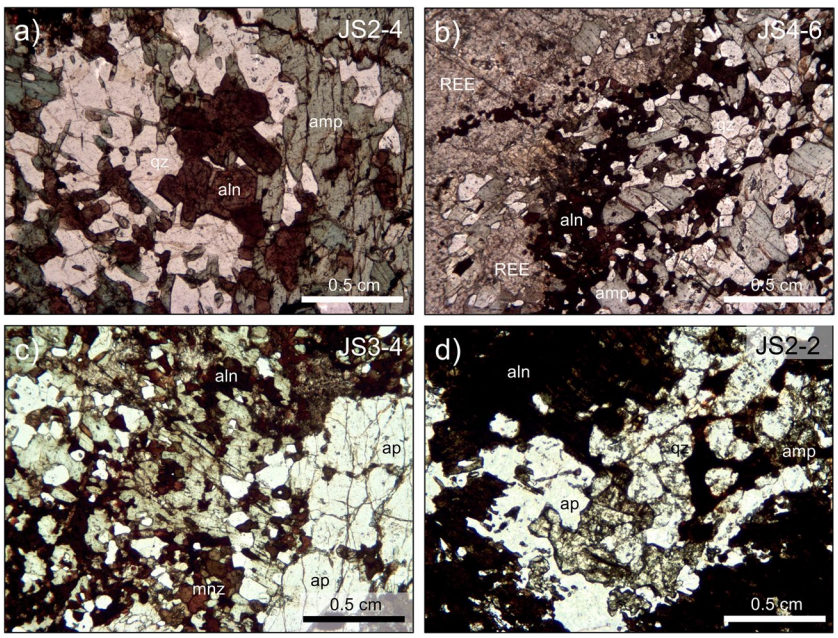

Fig. 10 Photomicrographs of four samples of green tinted amphibole-bearing rocks consisting of dark (hornblende) to pale (actinolite) green amphibole (ESM2 Table 4), allanite-(Ce), quartz, apatite and variable amounts of aggregates of lavender colored REE minerals, in some cases surrounded by allanite-(Ce) rims. (amp = amphibole; ap = apatite)

colored aggregates increases to greater than 50 vol. % and the amphibole-bearing rocks appear as the segregations in these aggregates. Neither plagioclase nor mica occur in any of these amphibole-bearing rocks.

The amphiboles vary in color and composition from dark green Mg-hornblende to pale green actinolite (ESM2 Table 4). The bulk compositions of these amphibole-bearing rocks (ESM1) varies from less than to greater than 50 wt. % SiO_2 depending on the amount of quartz relative to that of the REE mineral in the rock. Similar to the lavender REE-rich aggregates, these rocks have low La/Yb ratios and curved normalized REE patterns with lower light REE compared to middle REE (Fig. 5c). Compared to the parental magma in the northern locality (Table 2; Stern et al. 2018), the average composition of the amphibole-bearing rocks has lower La, but all the other REE are higher in concentration (Table 2) and the average La/Yb ratios lower than the bulk parental magma of the REE occurrence in the north. Also, SiO_2, Al_2O_3 and Na_2O are lower and Fe_2O_3, MgO and CaO higher in the amphibole-bearing rocks than the parental magma for the northern locality (Table 2), and based on their compositions the amphibole-bearing rocks do not appear to be crystallized equivalents of any common magma type.

New Locality

Approximately 150 meters north of the southern locality a previously unreported 2 m by 2 m outcrop of dark allanite-(Ce)-rich rocks was encountered (location m in Fig. 1). This consists of massive allanite-(Ce), monazite-(Ce), minor thorite and quartz. No other REE minerals were found at this locality. Allanite-(Ce) from this new locality has Al_2O_3 higher and Fe_2O_3 lower than allanite-(Ce) from the southern locality (ESM2 Table 2) and are more similar to allanite-(Ce) from the northern locality with respect to these elements. However, their La_2O_3 and Ce_2O_3 contents are similar to the allanite-(Ce) from the southern locality. Monazite-(Ce) at this locality has La_2O_3, Ce_2O_3, Nd_2O_3 similar to the northern locality, with La_2O_3 and Ce_2O_3 higher and Nd_2O_3, Sm_2O_3 and Y_2O_3 lower than monazite from the southern locality (ESM2 Table 3).

Felsic rocks

Small quartz-rich segregations within dark allanite-(Ce) nodules (Fig. 2b) and in allanite-(Ce) rims around lavender REE mineral aggregates (Fig. 2d) are spatially and unequivocally genetically related to the REE mineralization as they are fully contained within the allanite-(Ce) nodules. These segregations consist of granular quartz and sulfides (pyrite and chalcopyrite), in some cases intergrown with allanite-(Ce). They are unlike the aplites in the northern locality in that they have no feldspars. Due to their small size (generally <1 cm) they are difficult to extract from the surrounding allanite-(Ce), but whole-rock analysis of one sample (sample JS5-5B; ESM1), which also contains a small amount of amphibole, has high SiO_2, Fe_2O_3 and S and low Al_2O_3, Na_2O and K_2O reflecting the abundance of quartz and sulfides and lack of felspar in the rock. This sample has higher REE content than average aplite from the northern locality, with low normalized light REE relative to middle REE (Fig. 5d), very

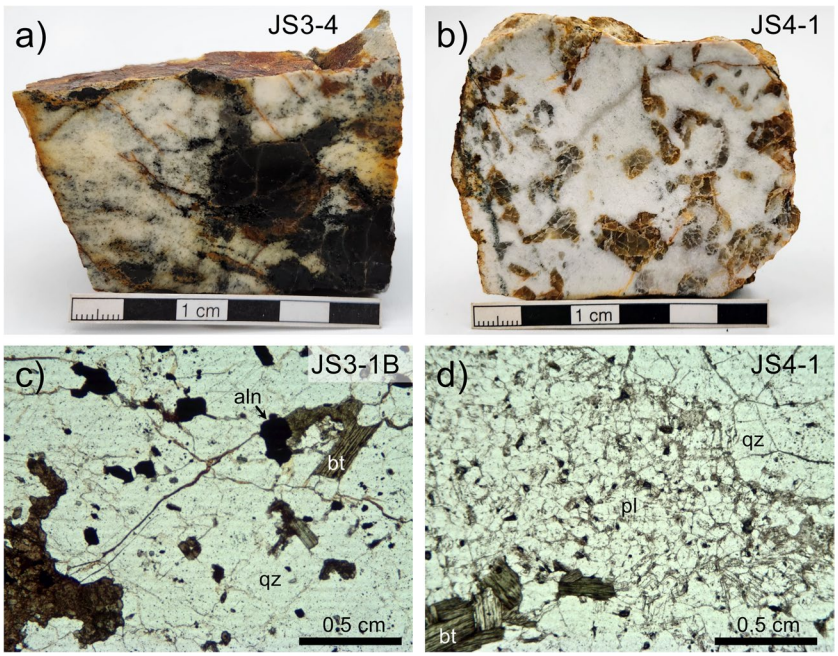

Fig. 11 Photos and photomicrographs of felsic rock samples JS3-4 and JS4-1 with large quartz phenocrysts in a fine grain aplitic groundmass of quartz, plagioclase, and green biotite

similar to some amphibole-rich samples despite its significantly different mineralogy.

Unequivocal aplite cogenetic with the REE mineralization also occurs as dikelets cutting lavender colored REE-rich aggregates. These dikelets consist of quartz, plagioclase partially altered to sericite, monazite-(Ce) and minor allanite-(Ce). Similar dikelets also occur cutting aggregates of REE minerals and aplite in the northern locality.

Larger bodies of felsic rocks that may be genetically related to the REE mineralization, and which occur in direct contact with REE mineralized rocks, consist of large quartz phenocrysts in a fine grained aplitic groundmass of quartz, altered feldspars and green biotite mica (Fig. 11). This groundmass resembles the aplites from the northern locality, but these latter lack large quartz phenocrysts. The green biotite in these rocks lack zircon inclusions and have higher MgO >10 wt. % and lower TiO_2 <2 wt. % (ESM2 Table 1) than the brown biotite in either the Idaho Springs Group metasedimentary mica schists or Longs Peak granites and pegmatites, as do the biotites in the aplites from the northern locality (Stern et al. 2018). The bulk whole-rock chemistry (ESM1) and REE content (Fig. 5d) of these samples is variable, but unlike the granular quartz- and sulfide-rich and plagioclase-free segregations described above, they have higher Al_2O_3 and Na_2O, reflecting the presence of plagioclase, but low K_2O reflecting the absence of alkali feldspar and/or muscovite. Their K_2O and Rb contents are also lower that than the metasedimentary mica schists of the Idaho Springs Group, which commonly contain alkali feldspar and muscovite. They have average lower REE content and La/Yb ratios than aplites from the northern locality, their La/Yb being similar to that of the lavender REE mineral aggregates and the amphibole-bearing rocks in the southern locality (Table 2; ESM1).

Age of the REE minerals

Ten allanite-(Ce) and four monazite-(Ce) grains analyzed from the three samples JS4-8, JS1-2, and JS1-9 indicate an age of 1421.9 ± 24.4 Ma (Fig. 12a). The data plot as two distinct clusters, one with lower $^{147}Sm/^{144}Nd$ (0.035 to 0.061) defined by the seven allanite-(Ce) and monazite-(Ce) grains from samples JS4-8 and JS1-9, and the other with higher $^{147}Sm/^{144}Nd$ (0.078 to 0.097) defined by the seven allanite-(Ce) and monazite-(Ce) grains from sample JS1-2. When bulk-rock Nd-isotopic data of two additional southern locality samples (allanite-(Ce) sample S1(Y) and REE mineralized sample SL1-3; Stern et al. 2018) are included, an age of 1444.1 ± 21.3 Ma is determined (ESM4 and ESM5). These ages agree with the electron microprobe U-Th-Pb ages of 1420 ± 25 Ma for monazite-(Ce) and 1442 ± 8 Ma for uraninite from the northern locality (Allaz et al. 2015).

Figure 12b plots initial Nd-isotopic compositions (at 1422 Ma) versus $^{147}Sm/^{144}Nd$ ratios for the 14 allanite-(Ce) and monazite-(Ce) grains analyzed from the three samples of the

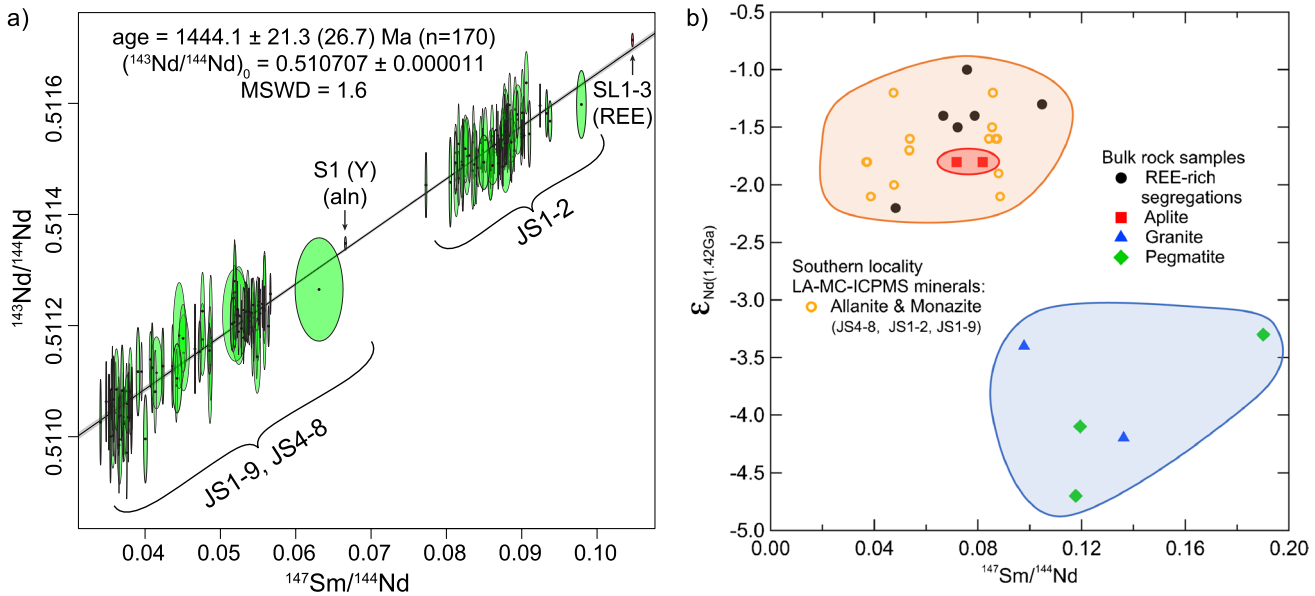

Fig. 12 **a** Nd-Sm isochron based on laser ablation of allanite-(Ce) and monazite-(Ce) grains in three samples from the southern locality (ESM4). **b** Plot of initial Nd-isotopic compositions (at 1422 Ma) versus $^{147}Sm/^{144}Nd$ ratios determined by laser ablation for the 14 allanite-(Ce) and monazite-(Ce) grains from the three samples of the southern locality (ESM4) compared to the initial isotopic Nd-isotopic compositions of bulk-rock samples of REE mineralization, aplite, granite, pegmatites and metasedimentary rocks from the northern locality (Stern et al. 2018)

southern locality (ESM4) compared to the initial isotopic Nd-isotopic compositions of bulk-rock samples of REE mineralization, aplite, granite, pegmatites and metasedimentary rocks from the northern locality (Stern et al. 2018). Together the grains analyzed yield $\varepsilon_{Nd1.42Ga}$ values that ranges from -1.2 to -2.1, with an average value of -1.7, similar to the northern locality aplite and REE mineralized segregations that have $\varepsilon_{Nd1.42Ga}$ values from -1.0 to -2.2, with an average of -1.6. In contrast, these values are distinct from the Longs Peak granites and granitic pegmatites in the area of the REE localities (Stern et al. 2018).

Discussion

The three outcrops of REE mineralization, which occur only ~1 km apart from each other near Jamestown, Colorado, are distinctive and globally unusual magmatic REE occurrences (Allaz et al. 2015), in the sense that all other known localities with significant fluorbritholite are associated with alkaline (Della Ventura et al. 1999; Liferovich and Mitchell 2006; Pekov et al. 2007; Vasyukova and Williams-Jones 2014, 2016, 2020), peralkaline (agpaitic; Jiexiang et al. 1994; Sørensen 1997) and carbonatite intrusions (Feldman et al. 1987), or are skarn-related occurrences such as in either the Bastnäs-type Bergslagen mining region of Sweden (Holtstam and Andersson 2007; Holtstam et al. 2014; Sahlström et al. 2019) or the IOCG-type Sin Quyen deposits of northwest Vietnam (Li and Zhou 2018). In contrast the magmatic deposits near Jamestown are spatially associated with the peraluminous Silver Plume-type granitic intrusions of the Longs Peak batholith. They are clearly not skarn-related as they have intrusive contacts into this granite and the metasedimentary schists of the Idaho Springs Group, which lack carbonate rocks (Fig. 1).

The two localities originally identified by Goddard and Glass (1940) are similar in both age and initial $\varepsilon_{Nd1.42Ga}$ values, indicating an isotopically similar magmatic source (Table 1). Their main REE mineral constituents fluorbritholite-(Ce), allanite-(Ce), monazite-(Ce), bastnäsite-(Ce), törnebohmite-(Ce) and uraninite are identical, although the southern locality also contains a Y-rich REE silicate mineral that was not observed in the north. In both localities, small globular aggregates of fluorite and monazite-(Ce) (Fig. 7) are observed, which indicate a melt immiscibility event in which an F-, P-, and REE-rich liquid separated from a more SiO_2 rich magma.

However, several important textural, mineralogical and compositional differences between the two occurrences stand out (Table 1). Most significantly, the lavender REE mineral aggregates in the southern locality have lower modal abundance of fluorite and lower F and Ca contents, higher Fe_2O_3, and do not exhibit the globular textures indicative of formation by melt immiscibility as observed in the northern locality (Fig. 2). Instead, two other important REE-rich lithologies, one consisting of almost pure allanite-(Ce) along with quartz, and another consisting of amphibole, allanite-(Ce), quartz, apatite, and variable amounts of other REE minerals, occur in the southern but not the northern locality. Also, the quartz phenocryst-rich felsic rocks that are spatially associated with, but do not host the REE mineralization in the southern locality, have higher SiO_2, more quartz and lower REE contents and La/Yb ratios, and thereby differ from the aplite that hosts the REE-rich globular segregations in the northern locality.

Although Goddard and Glass (1940) described the southern locality as a small outcrop of a lenticular vein "about 8 inches wide bordered by aplite on one side and by aplite grading into schist on the other", the multiple lithologic components revealed at depth indicate that the occurrence at this locality is clearly more complex. The implication is that although the formation of the globular REE-rich segregations hosted in aplite in the northern locality can be attributed to a process of fluoride-silicate melt immiscibility following ascent, cooling, and decompression of what was initially a single homogeneous silicate magma (Stern et al. 2018), the formation of the multiple REE-rich lithologies and their associated felsic rocks in the southern locality must have involved additional processes.

A number of conclusions can be inferred with some degree of certainty concerning the formation of the REE-rich lithologies in the southern locality. First, the presence of small globular aggregates of fluorite and monazite-(Ce) (Fig. 7) in both the southern and northern localities indicates that the immiscible separation of an F-, P-, and REE-rich liquid did occur at some stage in the formation of both these magmatic deposits. Although the lavender aggregates of REE minerals in the southern locality, which are similar in their mineralogic components to the centers of the REE-rich globular aggregates in the northern locality, have notably less fluorite and lower F content than these globules in the northern locality (Table 2), the high F and fluorite concentrations in the small fluorite and monazite-(Ce) segregations (Fig. 7) indicates that F was in fact an important component in the parental magmas that formed both occurrences. Although fluorite does occur in low abundance within the lavender REE segregations and in the amphibole-bearing lithologies in the southern locality it appears that much of the F that may have been initially present in the parental magma from which this occurrence formed has escaped. This may have been due to its volatility during crystallization and solidification of the different REE-rich lithologies. Nevertheless, the evidence for the presence of F in this parental magma—as preserved in the small fluorite plus monazite-(Ce) globular

segregations—is significant, since F is an essential element for facilitating the separation by melt immiscibility of an REE-rich component from a silicate magma (Veksler 2004; Stern et al. 2018). The apparent loss of F from the magmatic system of the southern locality might also have been one of the factors that led to the formation of amphibole and apatite as a repository for the Ca that in the northern locality is accommodated as fluorite.

Second, although the lavender REE mineral aggregates in the southern locality have higher heavy REE contents and lower La/Yb ratios than the mineralogically similar cores of the globular REE-rich segregations in the northern locality, the massive dark allanite-(Ce) nodules in the southern locality have lower heavy REE contents and higher La/Yb ratios than the allanite-(Ce) rims around the globular segregations in the north. Taken together the bulk average REE content and La/Yb ratio of the allanite-(Ce) and lavender REE-rich segregations in the south (Table 2) are similar to those of the bulk globular segregations in the northern locality (Fig. 8c). This suggests that a similar petrogenetic process was involved in both locations to form these two lithologies, namely immiscible separation of an F-, P-, and REE-rich melt from a silicate magma, followed by the subsequent crystallization of the allanite-(Ce) to form, by crystal-liquid fractionation, the even more heavy REE-enriched lavender REE mineral segregations (Stern et al. 2018). Fluoride-silicate melt immiscibility has also been shown to play an important role in the formation of REE-rich ores in a number of other locations worldwide (Andreoli et al. 1994; Vasyukova and Williams-Jones 2014, 2016, 2020; Van Lichtervelde et al. 2021).

Thirdly, we suggest that the absence of the concentrically zoned globules that provide textural evidence in the northern locality (Fig. 2a) for this two-stage process of immiscible separation of an REE-rich melt from a silicate magma followed by the subsequent crystallization of allanite-(Ce), may have resulted from the southern locality solidifying more slowly (Table 1), possibly in a larger magma volume or at a somewhat greater depth, allowing a greater degree of separation and agglomeration of these different phases. Rapid quenching and crystallization must have occurred in the northern locality to preserve the globular textures of the REE-rich immiscible melts within their host aplite (Fig. 2a). Somewhat slower solidification of the system in the southern locality might also explain the loss of F from the REE-rich immiscible melt segregations. The new locality (m; Fig. 1) we encountered also consists of massive allanite-(Ce) and presuming that it formed in a similar fashion to the southern locality it may be associated with aggregates of other REE minerals not exposed at the surface.

Finally, determining the andesitic composition of the parental magma in the northern locality (Table 2) was readily possible by analyzing large bulk samples of aplite and REE-rich globular segregations, since these two products of the immiscible separation of the REE-rich components from the SiO_2-rich aplite were spatially preserved together (Fig. 2a; Stern et al. 2018). In the southern locality the situation is more complex, since the lavender REE-mineral rich aggregates, dark allanite-(Ce) nodules, amphibole-bearing rocks and possible genetically related felsic rocks, although all spatially associated, occur as separate units and their relative proportions cannot readily be estimated. It is certainly clear that the amphibole-bearing rocks, which have average SiO_2 content of 54 wt. %, similar to a mafic andesite, are not simple a solidified equivalent of a parental magma, since they have significantly lower Al_2O_3, Na_2O and K_2O compared to any normal magmatic compositions. It is more plausible that these amphibole-bearing rocks, which also contain allanite-(Ce), other REE minerals, fluorite, apatite and quartz, crystallized from the relatively silica-rich melt complimentary to the lavender REE mineral rich and dark allanite-(Ce) rich rocks after the immiscible separation of these latter components from the parental magma. If this parental magma was similar to that in the northern locality, the crystallization of the amphibole-bearing rocks would have produced a residual magma even more silica-rich than the aplites of the northern locality, and in fact this is what is observed in the almost pure quartz segregations and quartz phenocryst-bearing high-silica (Table 2) felsic rocks we suggest to be co-genetic with the REE mineralization in the south. The occurrence of the CaO, Fe_2O_3, and MgO rich amphibole-bearing rocks, and the higher Fe_2O_3 content of both the lavender REE mineral rich segregations and dark allanite-(Ce) nodules compared to the globular REE segregations in the northern locality, together suggests that the parental magma for the southern locality was possibly more mafic than that of the northern locality, consistent with a higher degree of partial melting of the isotopically similar mafic or ultramafic source proposed for the northern locality (Stern et al. 2018).

Conclusions

In summary, we conclude that the southern locality formed by a complex sequence of igneous processes at essentially the same time (1.42(2) Ga) as the northern of the two magmatic REE occurrences near Jamestown, Colorado, and that their parental magmas were derived by melting of an isotopically similar mafic or ultramafic source in the lower crust or upper mantle (Stern et al. 2018). We suggest that during the rise, decompression and cooling of this silicate

magma, in association with its intrusion along the foliation of the metasedimentary biotite schists of the Idaho Springs Group, fluorite-silicate melt immiscibility caused the separation of small F-, P-, and REE rich melt globules that are still preserved as small spherical aggregates of fluorite and monazite-(Ce) in both occurrences (Table 1). Another melt immiscibility event further separated a REE-rich, silica-poor melt from a more silica-rich, REE-poor melt. Relatively slow cooling and crystallization of allanite-(Ce) from the REE-rich melt generated dark allanite-(Ce) rich rocks and lavender REE mineral aggregates in the southern locality. Together, these have total bulk average REE concentrations similar to the rapidly quenched concentrically zoned REE-rich globules in the northern locality, but with higher total Fe_2O_3, possibly because the parental magma was more mafic to begin with, and with lower total F because in the southern locality F escaped from the system as a volatile element. The loss of F limited the formation of fluorite, increasing the Ca content of the residual melt and leading to the crystallization of amphibole, which continued to removed Fe_2O_3, MgO, and CaO from the residual magma, resulting in the generation of the SiO_2 rich quartz phenocryst bearing felsic rocks associated with the REE mineralization. The discovery of a new massive allanite-(Ce) outcrop in the area increases the number, spatial distribution, and total volume of these globally unique magmatic REE deposits near Jamestown, Colorado.

Supplementary Information The online version contains supplementary material available at https://doi.org/10.1007/s00126-024-01291-2.

Acknowledgements MBR acknowledges Brian Walko for his support in locating the southern occurrence, and Yuan Yuan, Linus Raschke, and Simon Raschke for support in sampling and core drilling. We thank the Balarat Outdoor Education Center, Denver Public Schools, for providing site access to the northern locality. We thank Aaron Bell for support with the electron microprobe work and Lang Farmer for bulk Nd-Sm isotope analysis and valuable discussions. We acknowledge Kevin Mahan and Alexander Gysi for valuable discussions as well as two anonymous reviewers and the MD editor Karen Kelley for constructive suggestions. Financial support was provided by the Department of Physics, University of Colorado and the University of Electronic Sciences and Technology, Chengdu, through discretionary funds.

Author contributions Sample collection and preparation, data collection and analysis were performed by Charles Stern, Julien Allaz, Shea Burnham and Markus Raschke. LA-ICP-MS isotopic analysis were performed by Shea Burnham and Andrew Kylander-Clark. The first draft of the manuscript was written by Charles Stern and all authors commented on previous versions of the manuscript. All authors read and approved the final manuscript.

Declarations

Competing interests The authors have no competing interests to declare that are relevant to the content of this article.

References

Allaz J, Raschke M, Persson P, Stern CR (2015) Age, petrochemistry, and origin of a REE-rich mineralization in the Longs Peak, St. Vrain pluton, near Jamestown, Colorado (USA). Am Mineral 100(10):2123–2140. https://doi.org/10.2138/am-2015-5253

Anderson JL, Thomas WM (1985) Proterozoic anorogenic two-mica granites: Silver Plume and St. Vrain batholiths of Colorado. Geology 13:177–180. https://doi.org/10.1130/0091-7613(1985)13<177:PATGSP>2.0.CO;2

Andreoli MAG, Smith CB, Watkeys M, Moore JM, Ashwal LD, Hart RJ (1994) The geology of the Steenkampskraal monazite deposit, South Africa; implications for REE-Th-Cu mineralization in charnockite-granulite terranes. Econ Geol 89:994–1016

Baker F, Hedge CE, Millard HTJ, O'Neil JR (1976) Pikes Peak batholith: geochemistry of some minor elements and isotopes, and implications for magma genesis. In Professional Contributions of Colorado School of Mines: Studies in Colorado Field Geology 8: 44-56

Boos MF, Boos CM (1934) Granites of the Front Range-The Longs Peak-St. Vrain batholith. Geol Soc Am Bull 45:303–332. https://doi.org/10.1130/GSAB-45-303

Chakhmouradian AR, Wall F (2012) Rare earth elements: minerals, mines, magnets (and more). Elements 8:333–340. https://doi.org/10.2113/gselements.8.5.333

Chakhmouradian AR, Zaitsev AN (2012) Rare earth mineralization in igneous rocks: sources and processes. Elements 8:347–353. https://doi.org/10.2113/gselements.8.5.347

Cole JC, Braddock WA (2009) Geologic Map of the Estes Park 30' x 60' Quadrangle. US Geol Surv Science Investigation Map 3039:1

Della Ventura G, Williams CT, Cabella R, Oberti R, Caprilli E, Bellatreccia F (1999) Britholite-hellandite intergrowths and associated REE-minerals from the alkali-syenitic ejecta of the Vico volcanic complex (Latium, Italy): Petrological implications bearing on REE mobility in volcanic systems. Eur J Mineral 11:843–854

DePaolo DJ (1981) Neodymium isotopes in the Colorado Front Range and crust-mantle evolution in the Proterozoic. Nature 291:193–196. https://doi.org/10.1038/219913a0

Feldman IG, Sarkisyan SS, Boriskin VP, Purusova SP, Nguen VH, Chin SB (1987) Crystalline beckelite from Nam Se deposit (Northern Vietnam). Mineralogicheskiy Zhurnal 9:78–86 (in Russian)

Fisher CM, McFarlane CR, Hanchar JM, Schmitz MD, Sylvester PJ, Lam R, Longerich HP (2011) Sm–Nd isotope systematics by laser ablation-multicollector-inductively coupled plasma mass spectrometry: Methods and potential natural and synthetic reference materials. Chem Geol 284(1-2):1–20. https://doi.org/10.1016/j.chemgeo.2011.01.012

Flanagan FJ (1973) 1972 values for international geochemical reference samples. Geochim Cosmochim Acta 37:1189–1200 https://doi.org/10.1016/0016-7037(73)90055-0

Foster GL, Vance D (2006) In situ Nd isotopic analysis of geological materials by laser ablation MC-ICP-MS. J Anal At Spectrom 21(3):288–296. https://doi.org/10.1039/B513945G

Goddard E, Glass JJ (1940) Deposits of radioactive cerite near Jamestown, Colorado. Am Mineral 25(6):381–404

Holtstam D, Andersson UB (2007) The REE minerals of the Bastnäs-type deposits, south-central Sweden. Can Mineral 45:1073–1114

Holtstam D, Andersson UB, Broman C, Mansfeld J (2014) Origin of REE mineralisation in the Bastnäs-type Fe-REE-(Cu-Mo-Bi-Au) deposits, Bergslagen, Sweden. Mineral Deposita 49:933–966

Jiexiang G, Chao GY, Tang S (1994) Fluorbritholite-(Ce) A new mineral from Mont St. Hilaire, Quebec, Canada. J Wuhan Univ Technol (China) 9(3):9–14 (in Chinese with English abstract)

Kylander-Clark ARC (2010) Expanding the limits of laser-ablation U–Pb calcite geochronology. Geochronology 2:343–354. https://doi.org/10.5194/gchron-2-343-2020

Li X-C, Zhou M-F (2018) The Nature and Origin of Hydrothermal REE Mineralization in the Sin Quyen Deposit, Northwestern Vietnam. Econ Geol 113(3):645–673. https://doi.org/10.5382/econgeo.2018.4565

Liferovich RP, Mitchell RH (2006) Apatite-group minerals from nepheline syenite, Pilansberg alkaline complex, South Africa. Mineral Mag 70:463–484 https://doi.org/10.1180/0026461067050346

Paton C, Woodhead JD, Hellstrom JC, Hergt JM, Greig A, Maas R (2010) Improved laser ablation U-Pb zircon geochronology through robust downhole fractionation correction. Geochem Geophys Geosyst 11:Q0AA06. https://doi.org/10.1029/2009GC002618

Pekov IV, Pasero M, Yaskovskaya AN, Chukanov NV, Pushcharovsky DY, Merlino S, Zubkova NV, Kononkova NN, Menshikov YP, Zadov AE (2007) Fluorcalciobritholite, (Ca,REE)5[(Si,P)O4]3F, a new mineral: description and crystal chemistry. Eur J Mineral 19:95–103. https://doi.org/10.1127/0935-1221/2007/0019-0095

Peterman ZE, Hedge CE (1968) Chronology of Precambrian events in the Front Range, Colorado. Can J Earth Sci 5:749–756. https://doi.org/10.1139/e68-073

Peterman ZE, Hedge CE, Braddock W (1968) Age of Precambrian events in the Northeastern Front Range, Colorado. J Geophys Res 73(6):2277–2296. https://doi.org/10.1029/JB073i006p02277

Sahlström F, Jonsson E, Högdahl K, Troll VR, Harris C, Jolis EM, Weis F (2019) Interaction between high temperature magmatic fluids and limestone explains 'Bastnäs-type'REE deposits in central Sweden. Nat Res Sci Rep 9:15203. https://doi.org/10.1038/s41598-019-49321-8

Selverstone J, Hodgins M, Aleinikoff JN, Fanning CM (2000) Mesoproterozoic reactivation of a Paleoproterozoic transcurrent boundary in the northern Colorado Front Range: Implications for ~1.7- and 1.4-Ga tectonism. Rocky Mt Geol 35(2):139–162. https://doi.org/10.2113/35.2.139

Smith MP, Moore K, Kavecsanszki D, Finch AA, Kynicky J, Wall F (2016) From mantle to critical zone: a review of large and giant sized deposits of the rare earth elements. Geosci Front 7:315–334 https://doi.org/10.1016/j.gsf.2015.12.006

Sørensen H (1997) The agpaitic rocks—an overview. Mineral Mag 61:485–498. https://doi.org/10.1180/minmag.1997.061.407.02

Stern CR, Allaz JM, Raschke MB, Farmer GL, Skewes MA, Ross JT (2018) Formation by silicate-fluoride + phosphate melt immiscibility of REE-rich globular segregations within aplite dikes. Contrib Mineral Petrol 173:65. https://doi.org/10.1007/s00410-018-1497-7

Tweto O (1979) Geologic map of Colorado, special publication, scale 1:500,000. U.S. Geol Surv, Reston

Van Lichtervelde M, Goncalves PP, Eglinger A, Colin A, Montel JM, Dacheux N (2021) Solubility of monazite-cheralite and xenotime in granitic melts, and experimental evidence of liquid-liquid immiscibility in concentrating REE. J Petrol 62:1–20

Vasyukova O, Williams-Jones AE (2014) Fluoride–silicate melt immiscibility and its role in REE ore formation: Evidence from the Strange Lake rare metal deposit, Québec-Labrador, Canada. Geochim Cosmochim Acta 139:110–130

Vasyukova O, Williams-Jones AE (2016) The evolution of immiscible silicate and fluoride melts: Implications for REE ore-genesis. Geochim Cosmochim Acta 172:205–224

Vasyukova O, Williams-Jones AE (2020) Partial melting, fractional crystallization, liquid immiscibility and hydrothermal mobilisation – a 'recipe' for the formation of economic A-type granite-hosted HFSE deposits. Lithos 356-357:105300. https://doi.org/10.1016/j.lithos.2019.105300

Veksler IV (2004) Liquid immiscibility and its role at the magmatic-hydrothermal transition: a summary of experimental studies. Chem Geol 210:7–31

Wells JD (1967) Geology of the Eldorado Springs quadrangle Boulder and Jefferson counties, Colorado. 91 pp. U.S. Geol Surv Bull 1221-D